JSEE Vol. 26, No. 3, 2024 DOI: 10.48303/jsee.2024.2031006.1099

Research Paper

Seismic Retrofitting of Concrete Beam-Column Connections: Numerical Study FRP Strip and NSM Technique

Mohamad Reza Shokrzadeh[1*], Mahdi Sharifi[2] and Fariborz Nateghi Alahi[3]

1. Postdoctoral Researcher, International Institute of Earthquake Engineering and Seismology (IIEES), Tehran, Iran, *Corresponding Author; email: mr.shokrzadeh@srbiau.ac.ir
2. Assistant Professor, Department of Civil Engineering, Faculty of Engineering, University of Qom, Qom, Iran
3. Professor, Structural Engineering Research Center, International Institute of Earthquake Engineering and Seismology (IIEES), Tehran, Iran

Received: 07/06/2024
Accepted: 18/06/2024

Keywords:
Seismic Retrofitting; FRP; Concrete Beam-Column Connections; NSM

ABSTRACT

This study investigates cost-effective methods for retrofitting reinforced concrete joints using FRP (Fiber Reinforced Polymer) laminates and the NSM (Near-Surface Mounted) technique. Due to the high cost associated with preparing concrete surfaces and attaching FRP laminates, the study focuses on identifying optimal FRP strip configurations that minimize material use and surface preparation. Finite element modeling in ABAQUS revealed that a combined configuration of X-shape and orthogonal FRP strips achieves load-bearing capacities comparable to full FRP coverage, while reducing FRP material requirements by about 30%. Additionally, the study examined the performance of connections reinforced with FRP composites and CFRP rebars using numerical methods and laboratory results, assessing properties such as force-displacement curves, ductility, hardness, cracking, energy, and plastic strain. The findings demonstrate that the combined use of strip connections and the NSM method effectively enhances the structural performance of concrete beam-column joints, providing a practical and economical solution for seismic retrofitting.

How to cite the article:
Shokrzadeh, M. R., Sharifi, M., & Nateghi Alahe, F. (2024). Seismic Retrofitting of Concrete Beam-Column Connections: Numerical study FRP Strip and NSM Technique. *Journal of Seismology and Earthquake Engineering*, *26*(3), 25-40. DOI: 10.48303/jsee.2024.2031006.1099

1. Introduction

In the field of structural strengthening, several factors necessitate the reinforcement of structures. These factors include errors in calculation, design, and supervision, changes in the usage of the structure, increased demand for capacity, accidental loads, and changes in building codes (Shokrzadeh et al., 2024; Mostofinejad & Hajrasouliha, 2019). Therefore, strengthening the main load-bearing components of structures, such as reinforced concrete beams and columns, is crucial as these elements transfer axial and bending loads to the foundation. Additionally, for the proper performance of a reinforced concrete structure, the beam-to-column joint area and its sufficient strength are also very important. The beam-to-column joint area in moment-resisting frames plays a critical role and is considered one of the most critical locations for resisting seismic loads. Strengthening the joint areas of reinforced concrete structures through concrete and steel jackets has been one of the common methods in past decades. However, this method can be problematic and costly, requiring extensive equipment and labor (Han et al., 2023; Shokrzadeh et al., 2024). Moreover, adding concrete jackets increases the weight of the structure. Moreover, adding concrete jackets to the structure increases its weight, and steel jackets also face issues such as vulnerability to fire and buckling under axial stresses. Additionally, incomplete bonding between the steel jacket and the column surface during the initial loading stages can lead to weaknesses in confining the concrete of the column (Apandi et al., 2023; Shokrzadeh et al., 2023). In lateral load-bearing systems, the connections and their components must be strengthened in such a way that, after reinforcement, they possess appropriate stiffness, strength, and geometry. This ensures that the elastic behavior of the components provides the necessary conditions for the cyclic inelastic behavior of other members, maintaining the continuity of the load transfer path. This should be done in such a way that the plastic hinge forms at the appropriate locations at both ends of the beam, with adequate ductility, and outside the beam-to-column joint area (Ji et al., 2023; Shokrzadeh, 2017; Shokrzadeh et al., 2016). Cosenza et al. (Di Ludovico et al., 2008) and Balsamo et al. (Esmaeeli & Barros, 2015) conducted pseudo-dynamic experiments on a full-scale, three-story SPEAR model. This structure, initially designed solely for gravity loads, was retrofitted using FRP laminates. The retrofit involved comprehensive coverage of columns, beams, and joints. Their findings revealed that this retrofit method effectively enhanced the seismic performance of the reinforced concrete (RC) frame, increasing its seismic strength by 1.5 times when reinforced with CFRP (Carbon Fiber Reinforced Polymer) sheets. Karayannis et al. examined the behavior of exterior beam-column joints strengthened using a combination of epoxy resin injection and CFRP sheets. Twelve specimens were subjected to cyclic loading, and the results demonstrated notable improvements in both bearing capacity and ductility due to the retrofitting technique. Shrestha et al. (2009) investigated the use of FRP strips for retrofitting RC beam-column joints. Two configurations were tested: one with three horizontal FRP strips at the beam-column connection extending to adjacent beam faces, and another with two vertical strips at the joint extending to adjacent column faces. Experimental results indicated that FRP strips, as opposed to laminates, could also significantly enhance the strength of concrete joints. Le-Trung et al. (2010) explored the shear capacity of concrete beam-column joints strengthened with CFRP strips in L-shaped, T-shaped and X-shaped configurations. Eight specimens were tested, showing that wide CFRP strips notably improved ductility and shear capacity, with the X-shaped arrangement offering superior performance. Realfonzo et al.(Realfonzo et al., 2014) studied the retrofitting of RC beam-column joints with FRP, while Shokrzadeh & Nateghi-Alahi (2022) evaluated hybrid NSM-CFRP bars and FRP sheets for seismic rehabilitation of concrete bridge piers. Their experiments involved ten beam-column joint specimens reinforced with various FRP strip widths and arrangements. Some damaged specimens were re-retrofitted with FRP sheets. The results highlighted that combining FRP sheets and steel profiles significantly enhanced load-carrying capacity and ductility due to the confinement provided by steel profiles. In a comprehensive analytical study, Shokrzadeh et al. (2024) assessed

different FRP strengthening configurations for RC beam-column joints. The study focused on the performance of exterior concrete connections retrofitted with FRP strips as a cost-effective alternative to full FRP coverage. Numerical model results indicated that a combined X-shape and orthogonal FRP strip configuration could achieve load-bearing capacities comparable to full FRP coverage, reducing required FRP materials by approximately 30%, thus lowering costs and construction efforts for joint rehabilitation.

1.1. Research Significance

Due to the suitable and unique properties of Fiber Reinforced Polymer (FRP) composites, their use as Near-Surface Mounted (NSM) rebars and external sheets for strengthening reinforced concrete structures has become one of the widely used methods of retrofitting. Additionally, the excellent corrosion resistance of FRP composites is another advantage of using this method. Over the past three decades, numerous studies have been conducted on the use of FRP for strengthening and rehabilitating structures 6. However, the high cost of FRP materials and their implementation is one of the challenges in using them for structural retrofitting and strengthening. Therefore, this study aimed to reduce the costs of retrofitting and strengthening by using cross-arranged FRP sheets and various configurations of CFRP rebars with the NSM method. For this purpose, the damages to connections and the procedures for strengthening concrete joints with FRP strips were modeled using the ABAQUS finite element software. To verify the accuracy of the finite element models and validate them, experimental studies by Shrestha et al. (2009) were compared with similar samples created in the software. Subsequently, by modeling weak and strengthened connections and comparing their performance, the impact of various configurations of CFRP rebars using the NSM method on the seismic retrofitting of connections was examined. This paper provides a comprehensive description of the thorough analysis and discussion of the seismic behavior of RC beam-column joint. The main practical and design considerations are highlighted, while key response characteristics, such as stiffness, strength, ductility, concrete crack and failure modes, energy dissipation, dissipated energy capacities, are examined. This research provides some recommendations for the selection and use of configurations of CFRP rebars with the NSM method within the context of the results considered.

2. Model Validation

To validate the numerical models, data from the experimental study conducted by Shrestha et al. (Shrestha et al., 2009) was employed. This study involved retrofitting a selected concrete joint specimen with vertical CFRP strips. The experimental setup and the retrofitting methodology are depicted in Figures (1) and (2). The specimen was subjected to a load applied at the beam's end. The concrete used in the joint had a compressive strength of 25.4 MPa at 28 days. Longitudinal reinforcements were made of steel with a yield strength of 532 MPa, and the stirrups were made of steel with a yield strength of 332 MPa. The FRP used for retrofitting had an elastic modulus of 243 GPa. Figures (1) to (3) (Shrestha et al., 2009) provide an overview of the specimen and the arrangement of the FRP strips.

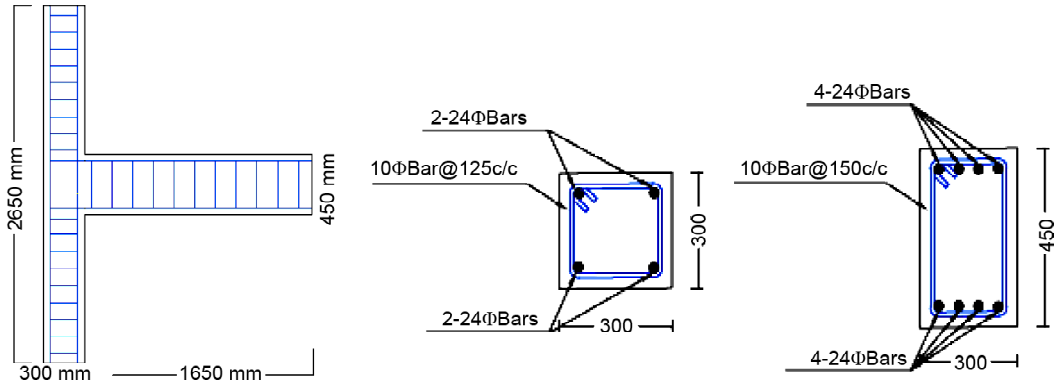

Figure 1. Schematic representation of the beam and column sections used in the verification model (Shrestha et al., 2009).

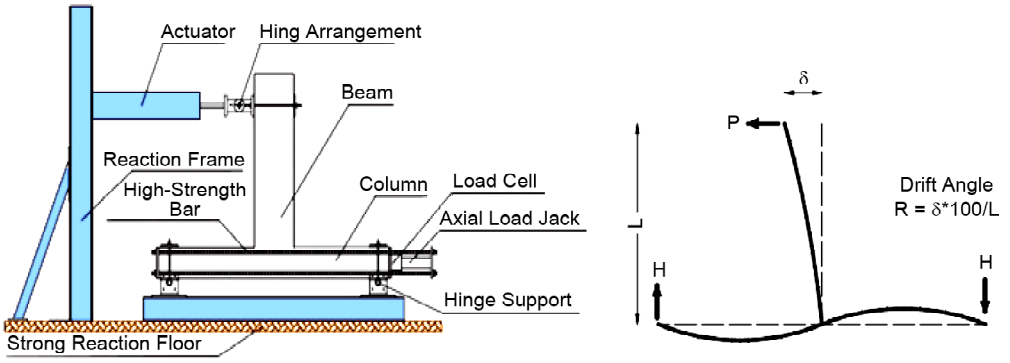

Figure 2. Configuration of loading and support for the experimental specimen (Shrestha et al., 2009).

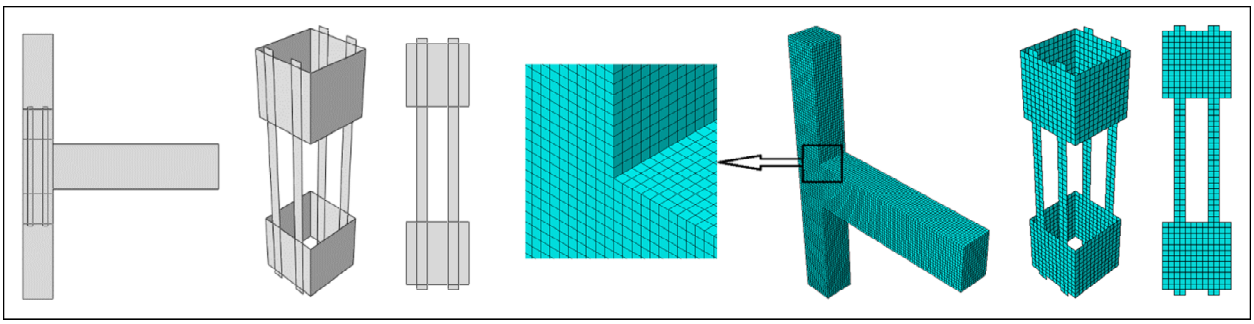

Figure 3. Arrangement of FRP strips as depicted in (Shrestha et al., 2009) and the mesh utilized in the verification model.

3. Numerical Models' Description

The finite element software ABAQUS was employed for modeling the experimental specimen. In simulating the beam-column joint, the Concrete Damage Plasticity (CDP) model was utilized to accurately represent concrete behavior within the finite element framework. This model integrates two primary failure modes of concrete: compressive crushing and tensile cracking (Shokrzadeh & Nateghi-Alahi, 2022). It combines isotropic elasticity degradation with compressive plasticity and isotropic tensile behavior. The chosen parameters include a Poisson's ratio of concrete set at 0.15 and a dilation angle (Ψ) of 36 degrees, which were determined through calibration (Shokrzadeh & Nateghi-Alahi, 2022). Furthermore, the modulus of elasticity of concrete was sourced from Equation (1) of ACI 318-19 (ACI 318-19, 2019).

$$Ec = 4700\sqrt{f'}\,(MPa)$$
$$(\text{in FPS unit } Ec = 57000\sqrt{f'}\,(psi)) \quad (1)$$

To describe the nonlinear uniaxial behavior of concrete, the Kent and Park models (Figures 4 and 5) were employed. In the Kent and Park

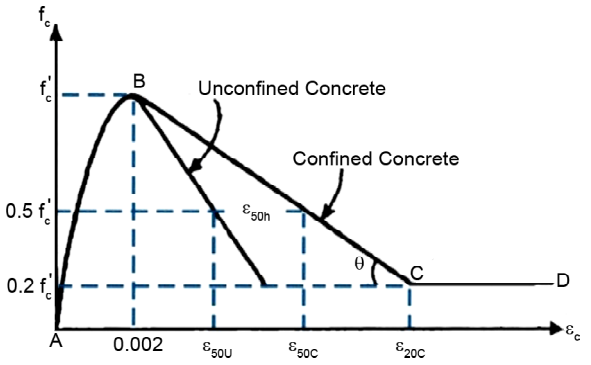

Figure 4. Comparison of stress-strain curves for unconfined and confined concrete specimens (Shokrzadeh et al., 2023).

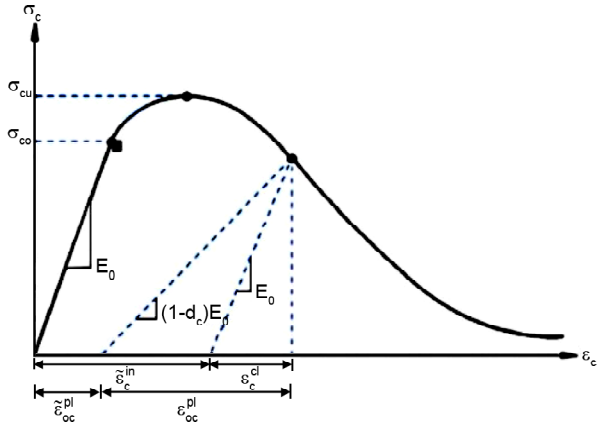

Figure 5. Illustration of the impact of compressive damage on the unloading slope during the compression phase (Shokrzadeh et al., 2022).

(1971) model, he calculation of compressive stress is governed by Equation (2):

$$\sigma_C = f'_{co}\left[2\left(\frac{\varepsilon_c}{\varepsilon'_c}\right)-\left(\frac{\varepsilon_c}{\varepsilon'_c}\right)^2\right] \quad (2)$$

where ε_c represents compressive strain, f_{co} denotes the compressive strength of the unconfined cylindrical concrete specimen, and ε'_c a is the corresponding strain, assumed to be 0.002 (Shokrzadeh et al., 2024; Shokrzadeh & Aziminejhad, 2018; Shokrzadeh & Nateghi-Alahi, 2022). Compressive stress is determined using the equation below (Shokrzadeh & Nateghi-Alahi, 2022):

$$\sigma_C = (1-d_c)E_O\left(\varepsilon_C - \varepsilon_C{}^{\sim PL}\right) \quad (3)$$

$$\varepsilon_C{}^{\sim PL} = \left(\varepsilon_C{}^{\sim in} - \frac{1}{(1-d_c)}\frac{\sigma_c}{E_0}\right) \quad (4)$$

where $\varepsilon_C{}^{\sim PL}$ represents inelastic strain, ε_C denotes compressive strain, E_0 is the elasticity modulus, d_c is compressive damage, and $\varepsilon_C{}^{\sim in}$ is the strain associated with damage. Equation 5 is utilized to compute the value of compressive damage (Shokrzadeh & Nateghi-Alahi, 2022):

$$dc = 1-\frac{\sigma_c}{f'_{co}} \quad (5)$$

where σ_c represents compressive stress and f'_{co} denotes the compressive strength of the unconfined cylindrical concrete specimen (Kent & Park, 1971; Shokrzadeh, 2024; Shokrzadeh et al., 2024; Vilanova et al., 2016; Sumer & Aktas, 2015). This model illustrates the influence of compressive damage on the unloading slope, as depicted in Figure (5) (Simulia & ABAQUS, 2019). To simulate the steel bars, two-node 3D truss elements (T3D2) were employed, along with four-node quadrilateral shell elements (S4R) for the FRP sheets, and eight-node solid elements (C3D8R) for the concrete. Mesh sizes varied according to the dimensions of each component (concrete, steel bar, and CFRP sheets). Following a mesh sensitivity analysis, a mesh size of 25 mm was chosen (Figure 3). The interaction between CFRP and concrete was modeled as perfectly bonded (tie). The interaction between concrete components and reinforcements was also modeled as perfectly bonded, with all reinforcements embedded in concrete (Kent & Park, 1971; Vilanova et al., 2016; Sumer & Aktas, 2015). The beam-column joint was supported at the top and bottom of the column, with displacement imposed at the beam end. The analysis was conducted using the implicit mode, and for quasi-static loading conditions, the static general method was selected for analysis.

Experimental testing of a beam-column retrofitted with carbon fiber strips and plates was conducted to validate the numerical model. The default *Kc* value of 0.667 provided the most accurate results for predicting ultimate capacity and failure mode. The dilation angle (Ψ) ranged from 25 to 35, and the viscosity parameter for concrete damage measurements was set at 0.001. Higher dilation angle values promoted ductile behavior, whereas lower values led to brittle responses. The compressive damage parameter (*dc*) significantly influenced the bending response of the hybrid structural elements. Choosing appropriate values for viscosity parameters is crucial in realistic simulations using the CDP material model. The values of 30 for dilation angle, 1.16 for viscosity, and 0.667 for *Kc* were found to best fit the experimental data (Shokrzadeh & Nateghi-Alahi, 2022). The concrete stress-strain behavior in compression and post-cracking tensile behavior were defined according to CEB-FIB guidelines. The developed numerical model accurately analyzed the experimental specimen. As depicted in Figure (6), the analytical results closely match the experimental findings.

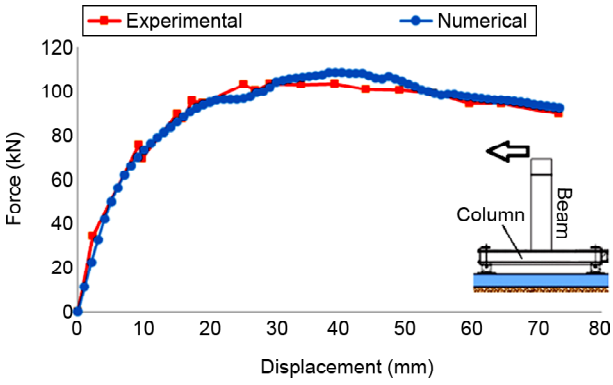

Figure 6. Comparison between the force-displacement curve obtained from experimental results (Shrestha et al., 2009) and numerical analysis results.

The maximum strength of the specimen, determined from the force-displacement curve (Figure 6), was 102.734 kN in the test. Numerically, this strength was estimated as 105.517 kN, indicating a numerical error of less than 5% compared to the experimental results in estimating member strength.

4 . Specimens Under Investigation

In this paper, various configurations of FRP strips are employed instead of complete FRP coverage to lower retrofit costs and reduce the surface preparation required. These configurations minimize the amount of FRP sheets used and decrease the preparation needed for attaching sheets to the concrete surface. To assess the effectiveness of these configurations, the initial joint specimen used for validation is retrofitted again and modeled with different strip arrangements.

4.1 Proposed FRP Retrofit Arrangements

In this study, various configurations of FRP strips are investigated to evaluate their performance compared to Specimen No. 1, which features complete coverage at the beam-column joint with maximum FRP usage and surface preparation. The detailed characteristics of each specimen configuration are outlined below:

a) Base Specimen without Retrofit: This specimen, illustrated in Figure (1), represents a vulnerable beam-column connection lacking joint stirrups and any retrofitting.
b) Specimen No. 1: Complete Wrapping: As depicted in Figure (7a), this specimen employs full FRP wrapping to reinforce the connection. The length of the retrofit area on the column face is *hc* (height of column section), and on the beam, it extends to one and a half times *hb* (height of beam section).
c) Specimen No. 2: Reduced Beam Retrofit with Complete Wrapping: Figure (7b) shows this specimen, where the retrofit length on the column face remains *hc*, while on the beam, it is half of *hb*.
d) Specimen No. 3: Complete Wrapping of Joint without Beam Retrofit: Shown in Figure (7c), this specimen features retrofitting along the entire column face (*hc*), omitting retrofitting on the beam.
e) Specimen No. 4: Diagonal and Three Horizontal Strips Retrofit Scheme: Figure (7d) displays this configuration, where the column face is retrofitted to *hc* length, the beam to half *hb* length, and the joint area with an X-shape and three horizontal strips each 0.05 m wide.
f) Specimen No. 5: One-Face Diagonal X-Shape and Two Orthogonal Retrofit Scheme: As seen in Figure (7e), this specimen retrofits the column face to *hc* length, the beam to half *hb* length, and employs three 0.05 m wide strips on the column sides and an X-shape with horizontal strips at the joint back.
g) Specimen No. 6: One-Face Orthogonal and Two Diagonal X-Shape Retrofit Scheme: Figure (7f) depicts this configuration, retrofitting the column face to hc length, half hb length on the beam, and using a combination of X-shape and horizontal strips on the column sides.
h) Specimen No. 7: X-Shape and Two Horizontal Strips Retrofit Scheme: Illustrated in Figure (7g), this specimen retrofits the column face to *hc* length, half *hb* length on the beam, and uses a combination of X-shape and horizontal strips at the joint area.
i) Specimen No. 8: Diagonal X-Shape Strips Retrofit Scheme: Shown in Figure (7h), this specimen retrofits the column face to *hc* length, half *hb* length on the beam, using an X-shape arrangement without horizontal strips.
j) Specimen No. 9: Two-Face Diagonal X-Shape and Two Orthogonal Strips Retrofit Scheme: Presented in Figure (7i), this configuration employs an X-shape arrangement on the column sides and two orthogonal strips at the joint back, with restrained full wrapping at the beam and column ends. The retrofit length on the column face is *hc*, and on the beam sides, it is half *hb*.

These configurations are studied to assess their effectiveness in reducing retrofit costs while maintaining structural integrity.

4.2 Investigation of Monotonic Force-Displacement Curves

To assess the performance of the specimens,

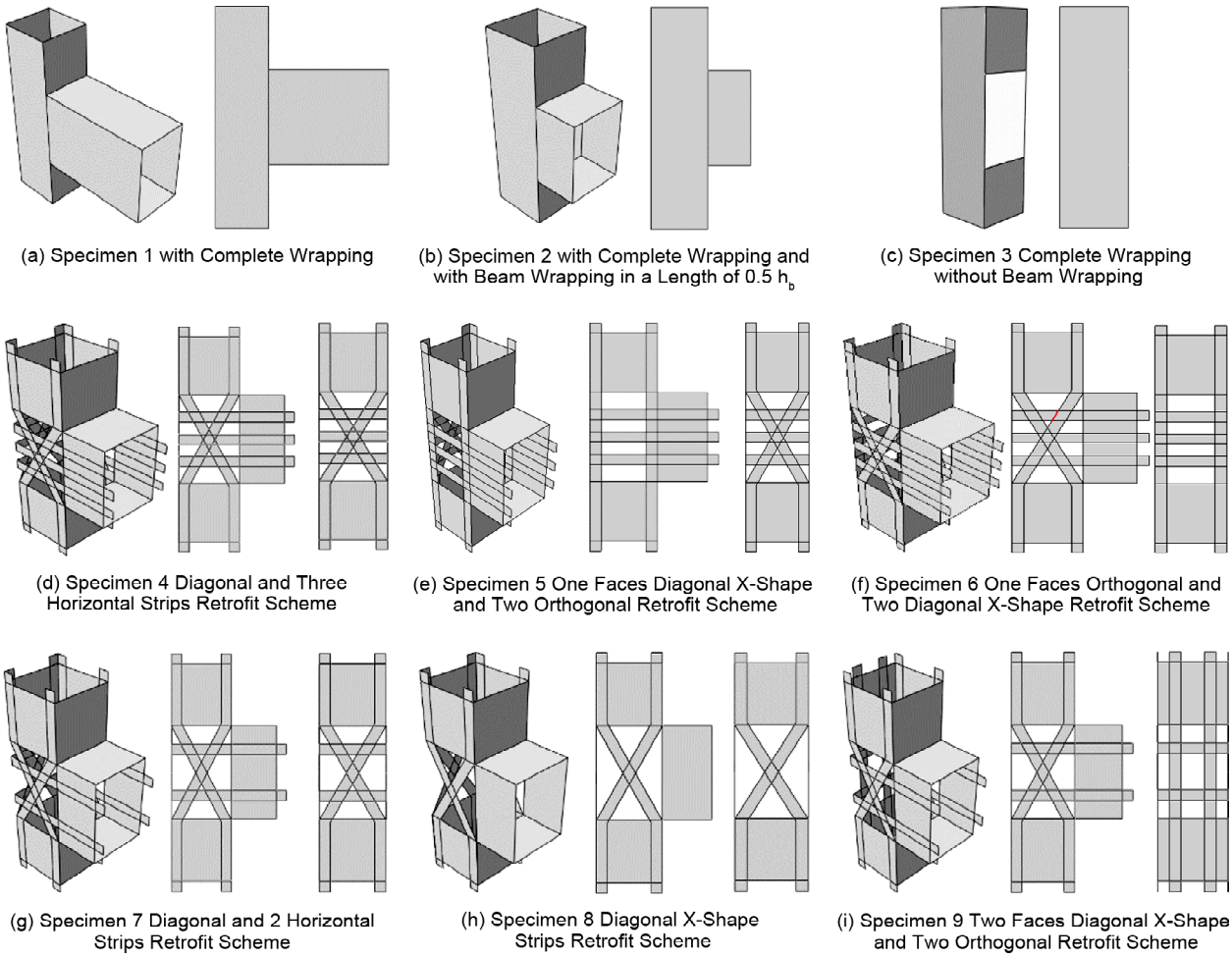

Figure 7. Various FRP retrofit arrangements in the considered specimens.

Table 1. The maximum load carrying capacity and the strength increase percentage for the retrofitted specimens and the base specimen.

Specimen	Maximum Strength (kN)	Drift Angle at the Maximum Capacity (%)	Deformation at the Maximum Capacity (mm)	Dissipated Energy (KN.mm)	Strength Ratio (Strength/Strength of Base Model)
Base	96.84	2.63	43.4	4651	-
1	144.28	5.44	61.56	13682	48.9
2	138	5.57	91.84	13168	42.5
3	130	2.63	43.4	12553	34
4	135.5	5.01	97.9	12890	40
5	127.6	6.67	110	12264	32
6	130.24	4.44	66.6	12600	34.5
7	126.7	4.16	68.6	12179	31
8	122.3	4.77	78.8	11875	26.2
9	131	3.36	55.5	12555	35.3

they underwent monotonic loading applied at the free end of the beam, and nonlinear static analyses were conducted. Figure (8) compares the force-displacement curves of the retrofitted specimens using FRP strips or laminates with those of the base model. These curves are also represented by idealized equivalent bilinear curves. Table (1) presents the ultimate strength values, percentage increase in strength compared to the base model, and the dissipated energy area beneath the force-displacement curve.

Among the different FRP strip arrangements, the full-coverage configuration exhibited the highest strength increase and energy dissipation

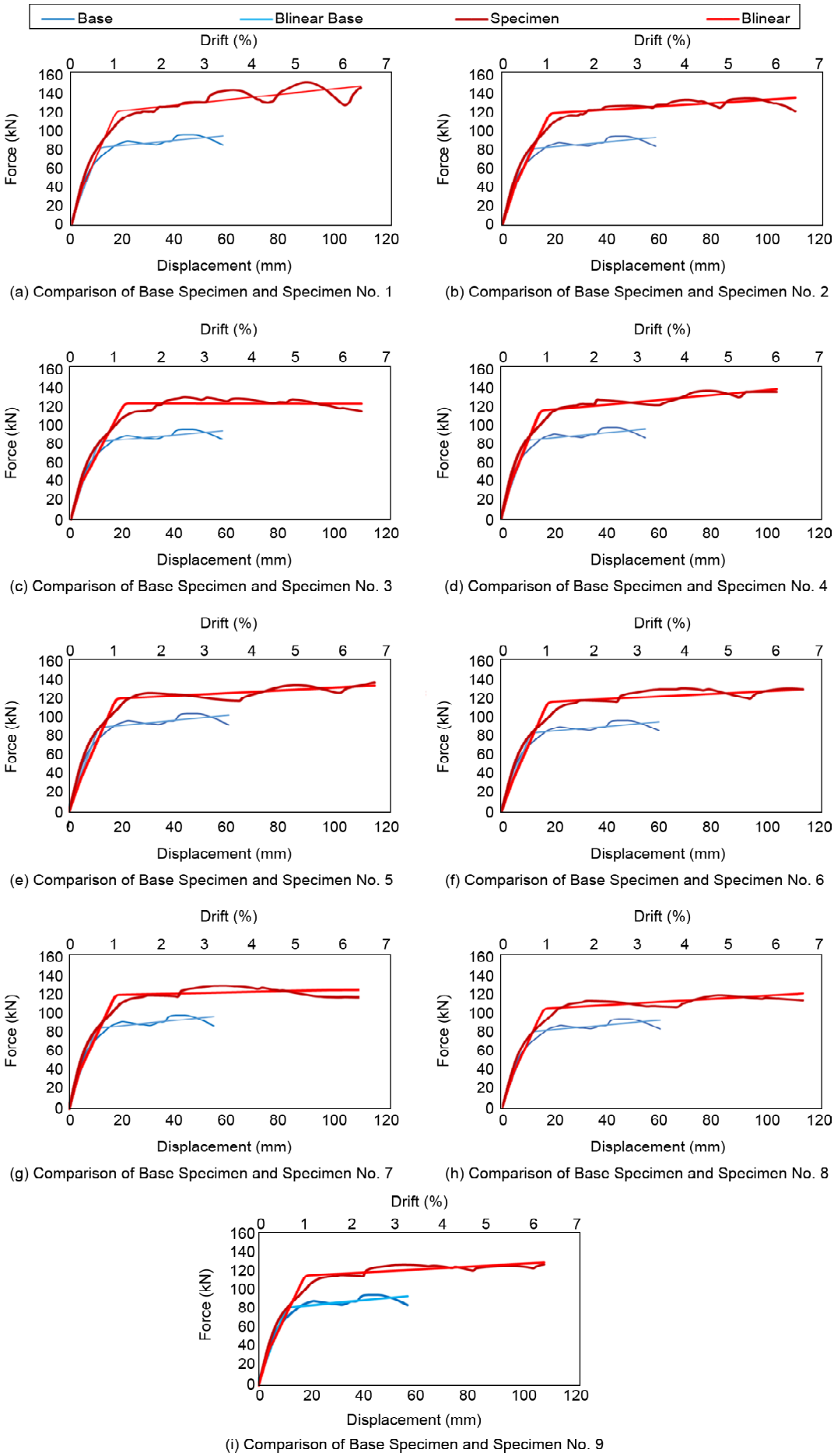

(a) Comparison of Base Specimen and Specimen No. 1

(b) Comparison of Base Specimen and Specimen No. 2

(c) Comparison of Base Specimen and Specimen No. 3

(d) Comparison of Base Specimen and Specimen No. 4

(e) Comparison of Base Specimen and Specimen No. 5

(f) Comparison of Base Specimen and Specimen No. 6

(g) Comparison of Base Specimen and Specimen No. 7

(h) Comparison of Base Specimen and Specimen No. 8

(i) Comparison of Base Specimen and Specimen No. 9

Figure 8. Comparison of Force-displacement and bilinear curves for retrofitted specimens and the base specimen.

capacity among the studied models. Among the strip configurations, Model No. 4, utilizing a combination of X-shape and three horizontal strips, demonstrated strength and energy dissipation closest to the full-coverage model, increasing the base model's strength by 40%. Model No. 5, employing orthogonal sheets on the sides without X-shaped strips, showed a 37% improvement in strength over the base model. However, the full coverage of the joint increased joint strength by 48.9% compared to the base model, indicating favorable performance of the strip models due to material savings, reduced removal of coverings and cladding materials, and simplified surface preparation.

Following this model, Model No. 9 with two orthogonal strips showed the next best performance. Model No. 8, which used only diagonal strips in the joint area, exhibited the lowest increases in strength and energy dissipation, improving the base model's strength by 26%.

4.3 Investigation of Ductility Ratio

Ductility refers to the capacity of a structural system to sustain substantial inelastic displacements while maintaining an acceptable decrease in its load-carrying capacity. This is quantified by the structure's overall ductility ratio (μ), which is derived from the idealization of its performance curve into equivalent bilinear curves representing elastic and perfectly plastic behavior.

According to equation (6), μ is calculated by dividing the maximum relative lateral displacement (*du*) by the relative yield lateral displacement (*dy*) (Shokrzadeh, 2017; Nateghi-Alahi & Shokrzadeh, 2019; Shokrzadeh et al., 2023). In specimens under consideration, relative lateral displacement is equal to deflection of beam end.

$$\mu = \frac{d_u}{d_y} \tag{6}$$

The displacement corresponding to a fraction of the peak load (*Fp*) can be considered the ultimate point. According to literature, this fraction typically ranges between 10% and 20% (Shokrzadeh et al., 2024; Shokrzadeh, 2017, 2024). Figure (9) illustrates an equivalent ideal bilinear diagram used to assess the ductility ratio. Both force-displacement and force-drift graphs are employed for the specimens, with corresponding values detailed in Table (2). In Table (2), deformations or displacements measured in millimeters (mm) are represented for the force-displacement graph, while drift angles or displacements resulting from drift are measured in millimeters (mm) for

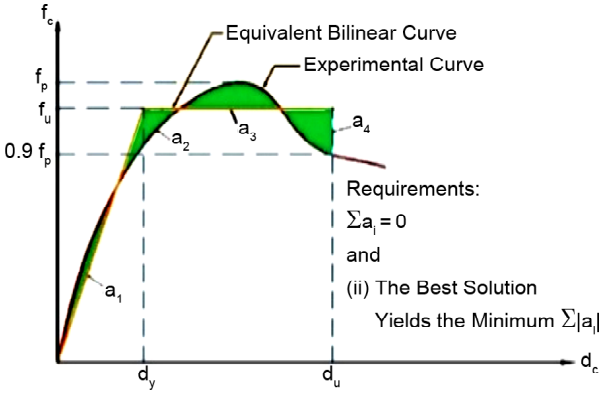

Figure 9. Equivalent bilinear curve definition for ductility ratio evaluation (Shokrzadeh & Nateghi-Alahi, 2022).

Table 2. Ductility ratio and related factors in retrofitted and base specimens.

Specimen	dy (Dic) & (Drift) (mm)	Du (Dic) & (Drift) (mm)	$\mu = \frac{d_u}{d_y}$	Increase of Ductility Ratio (%)
Base	11.1 (0.67)	57.52(3.49)	5.18	-
1	17.15 (1.04)	104 (6.24)	6.06	17
2	18.16 (1.1)	110 (6.67)	6.05	16.8
3	20.18 (1.28)	110 (6.67)	5.45	10.5
4	18.16 (1.1)	110 (6.67)	6.05	16.8
5	17.15(1.03)	110 (6.67)	6.41	23
6	17.15(1.03)	110 (6.67)	6.41	23
7	19.17 (1.16)	110 (6.67)	5.74	11
8	16.15 (0.98)	110 (6.67)	6.8	31
9	18.16 (1.1)	110 (6.67)	6.05	16.8

the force-drift graph. Values enclosed in brackets indicate uncertainties or variations in measurements. The table also includes the general ductility ratio (μ), maximum relative displacement (*du*), and relative yield displacement (*dy*) obtained from equivalent bilinear curves for all specimens. Most retrofitted systems reached a maximum drift limit of 6%. Specimen 6 exhibited the highest ductility ratio at this drift limit, despite entering the strength reduction region. Models 5, 6, and 8, retrofitted with configurations such as X-shape strip and horizontal strips, X-shape strips, and orthogonal strips, respectively, demonstrated the most favorable ductility characteristics. At a 6% drift, these models maintained their strength with minimal degradation.

4.4. The Maximum Plastic Strain Index

The maximum plastic strain index (PE) serves as a critical parameter for assessing concrete damage, particularly in evaluating the extent and progression of tensile and compressive failures (Shokrzadeh & Nateghi-Alahi, 2022).

Other parameters such as Tensile Damage Parameters (DAMAGET), Compression Damage (DAMAGEC), and Stiffness Determination (SDEG) also contribute to assessing concrete damage. However, *PE* holds significant importance in many applications and is widely utilized (Shokrzadeh & Nateghi-Alahi, 2022).

In the base specimen, the maximum plastic strain reaches approximately 8.9%, indicating extensive tensile damage in the concrete, predominantly concentrated around joints where crack formation is most anticipated. Figures (10) and (11) illustrate that FRP laminates and strips significantly enhance the shear capacity of the system, diverting cracks away from the joint region. However, in specimen No. 1, the maximum plastic strain rises to about 24.64% due to complete overlapping of the FRP, concentrating significant tensile damage in the concrete column. Specimen No. 3 exhibits a maximum principal plastic strain of 8.6%, attributed to inadequate cover at the beam

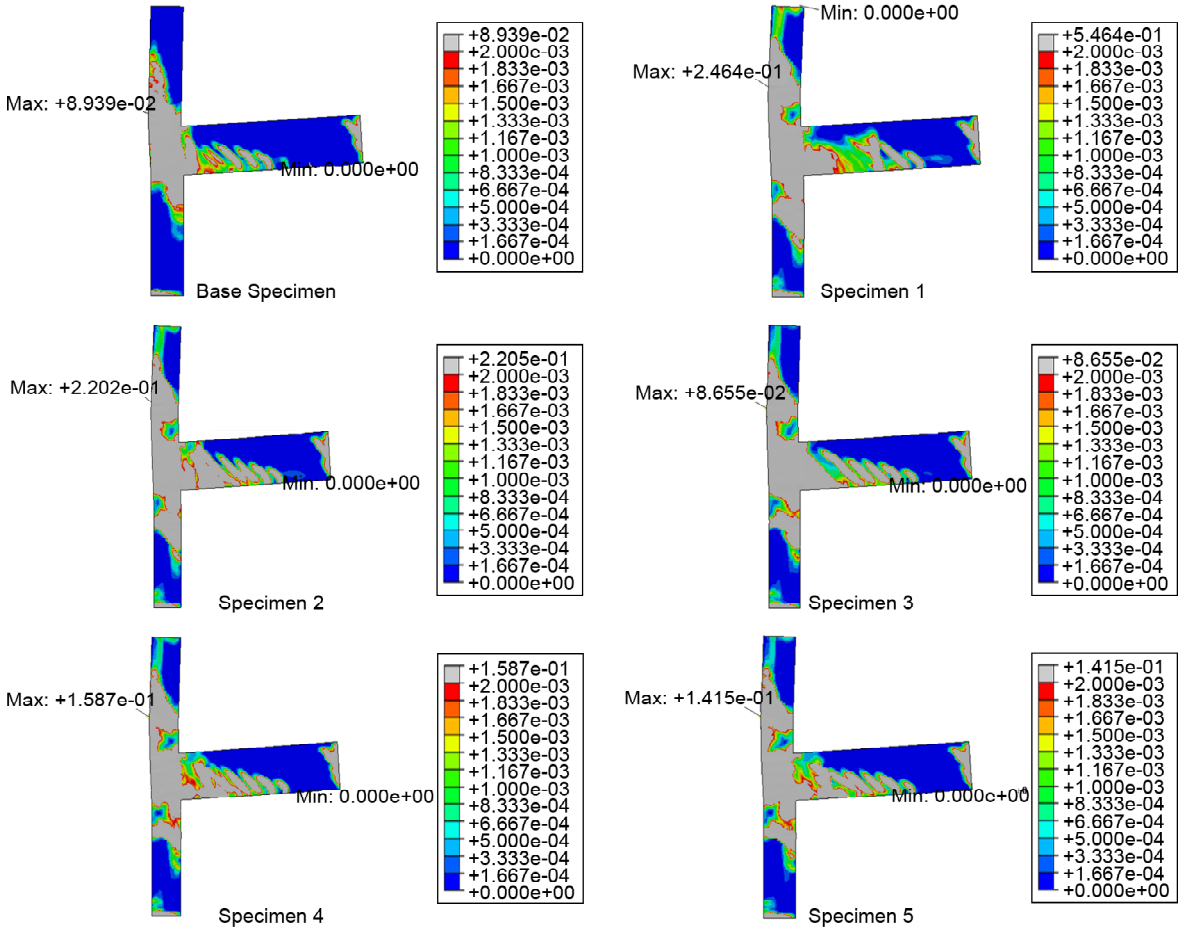

Figure 10. Comparison of maximum principal plastic strain in base and proposed specimens.

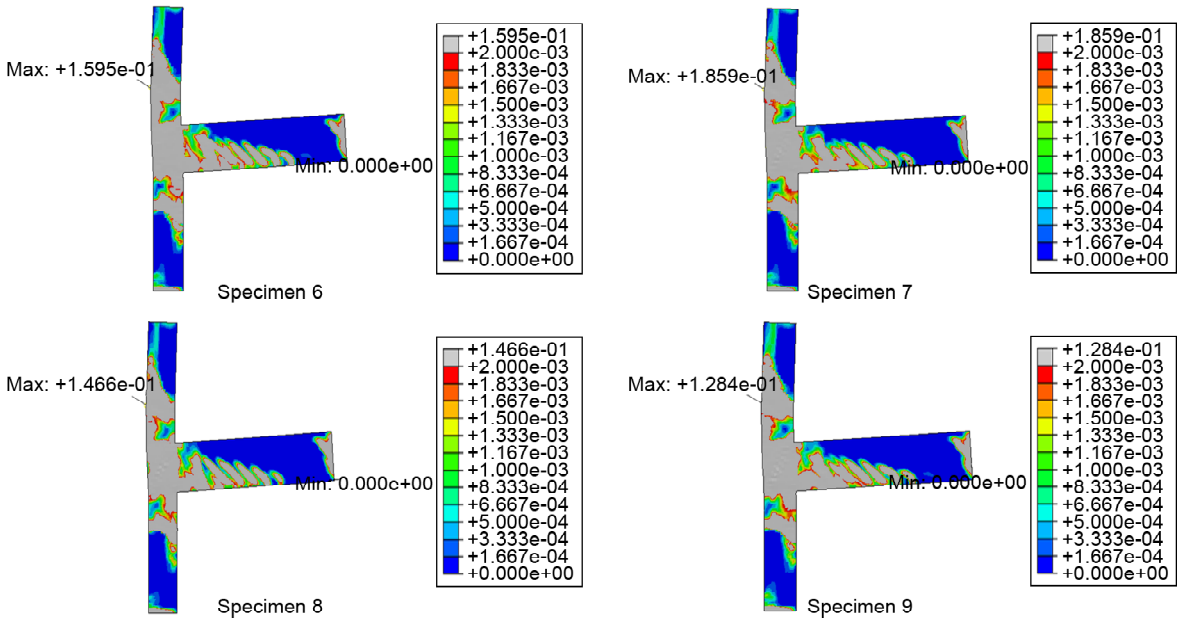

Figure 10. Continue.

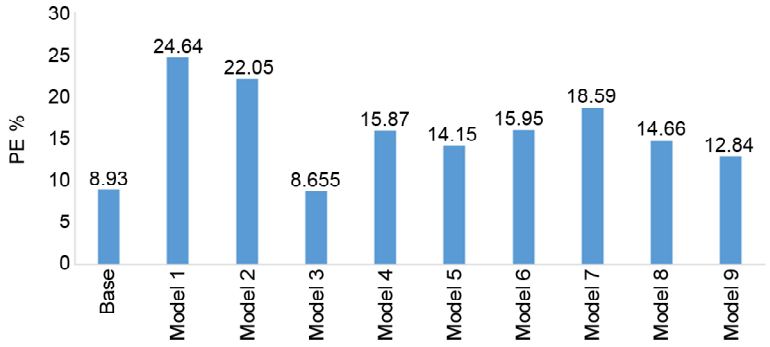

Figure 11. Maximum principal plastic strain of the specimen under consideration.

connection and alignment of generated cracks, potentially leading to plastic hinge formation on the connection face (Shokrzadeh et al., 2024, 2024; Shokrzadeh & Nateghi-Alahi, 2022). In specimen No. 9, the maximum principal plastic strain decreases to approximately 12.84% as expected, reflecting improved shear capacity. Specimens 1 and 2 demonstrate the highest strength increase due to extensive overlap of FRP, but this concentration of plastic strain in the column area increases damage at this critical section. Specimen No. 3 shows the least strength increase due to minimal overlap, correlating with a lower maximum plastic strain. Among strip-retrofitted specimens, specimen 9 exhibits relatively better performance. It achieves desirable strength enhancement while maintaining adequate ductility ratio. Plastic strains are effectively reduced and transferred to the concrete beam, thereby relocating the plastic hinge from the joint to the beam, making specimen 9 particularly suitable among strip-retrofitted specimens.

5. The Effect of FRP Strip and NSM Method on the Performance of the Retrofitted Joints

To comprehensively investigate the impact of various configurations of strip and Near Surface Mounted (NSM) methods on the performance of retrofitted joints, three specimens were analyzed at the beam-column junction. The specifications for these specimens, as detailed in Figure (12), include 50mm-wide FRP sheets uniformly applied with a thickness of 0.5mm across all configurations. As commonly cited in the literature, the predominant NSM method for reinforcing connections typically involves arranging FRP bars in the configuration depicted in Figure (12a). This arrangement is anticipated to significantly enhance resistance compared to the baseline (H sample). Furthermore,

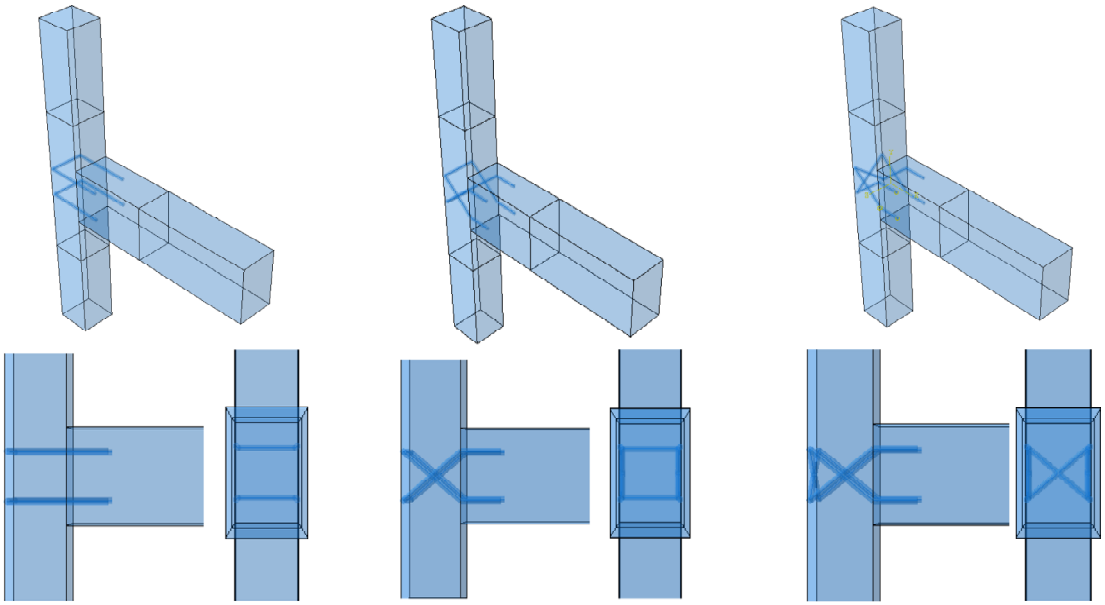

Figure 12. NSM arrangements in the specimens under consideration.

Figure (12b) illustrates an NSM method utilizing an X-shape and linear arrangement at the rear of the connection to enhance structural integrity. In contrast, Figure (12c) demonstrates an NSM approach using an X-shape configuration along the side and rear of the connection, showcasing the versatility of reinforcement strategies.

The performance of these retrofitted joints was evaluated based on their ability to mitigate crack propagation and improve overall structural resilience. The three specimens serve as critical case studies to assess how different NSM method geometries influence load distribution and deformation characteristics. By strategically deploying FRP materials in varied orientations and locations within the joints, the study aims to optimize both strength and ductility, essential for effective retro fitting applications. These findings provide valuable insights into the practical implementation of NSM techniques to enhance the seismic performance and durability of reinforced concrete structures.

5.1. Monotonic Behavior of Beam-Column Conection

To assess the performance of the specimens, they underwent monotonic deformation at the free end of the beam, and analyses were conducted using nonlinear static methods. Figure (13) presents a comparison of the load-displacement curves between the strengthened specimens and the No. 9 specimen. Each graph compares the load-displacement curve of one NSM method arrangement with that of the No. 9 specimen. To facilitate comparison, the load-displacement curves of the specimens are simplified using equivalent bilinear curves, as depicted in the figures. Table (1) provides details on strength values, percentage increase in strength, and the area under the load-displacement curve for the strengthened models. Figures (4a) to (4j) illustrate the comparison of these values for strength and energy dissipation across the specimens.

In specimen H-1, the maximum shear force sustained at the joint is 135 kN, marking an increase of approximately 0.7% compared to the No. 9 specimen. Specimen H-2 supports a maximum shear force of 138 kN at the joint, representing an increase of approximately 2.98% compared to the No. 9 specimen. Specimen H-3 sustains a maximum shear force of 139 kN at the joint, indicating an increase of approximately 3.73% compared to the No. 9 specimen.

5.2. Maximum Plastic Strain Index

In the No. 9 specimen (Figure 10), the maximum plastic strain is approximately 15%, indicating extensive tensile damage in the concrete, particularly at the joint where most of the cracks are concentrated. As expected and shown in Figure (14), the use of the NSM system significantly

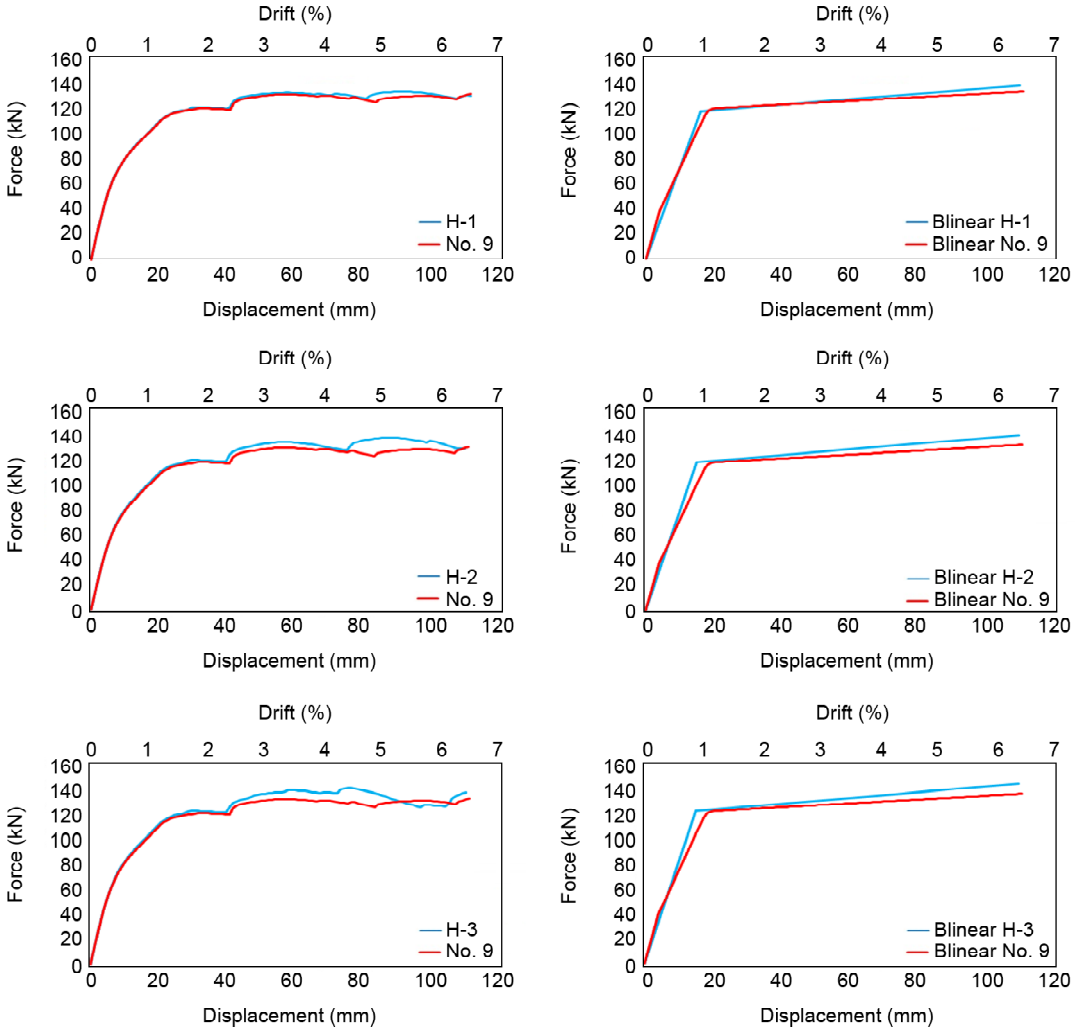

Figure 13. Comparison of Force-displacement and bilinear curves for retrofitted NSM specimens and the NO.9 specimen.

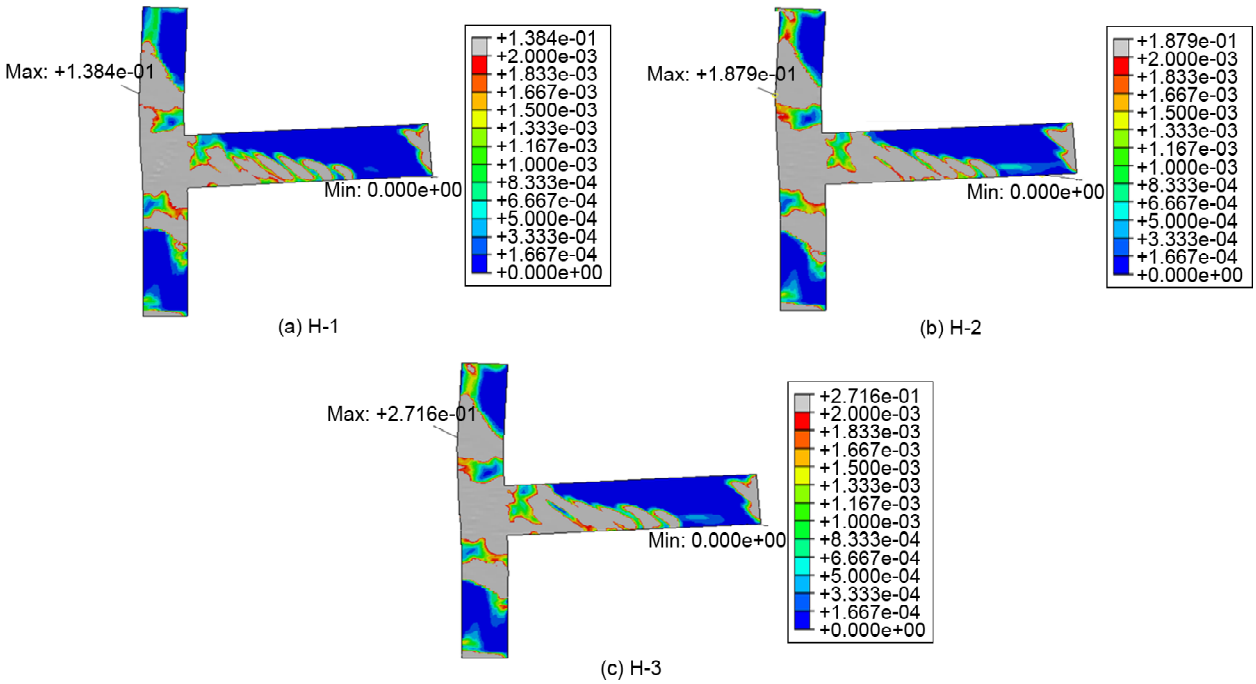

Figure 14. Maximum principal plastic strain in the proposed NSM specimens.

Table 3. The maximum load carrying capacity and the strength increase percentage for the retrofitted specimens and the base specimen

Specimen	Maximum Strength (kN)	Maximum Principal Plastic Strain	Drift Angle at the Maximum Capacity (%)	Deformation at the Maximum Capacity (mm)	Dissipated Energy (KN.mm)
No. 9	134	0.1286	5.44	91.56	12347
H-1	135	0.1384	5.57	91.84	12545
H-2	138	0.1879	5.63	93.4	12862
H-3	139	0.2716	5.01	97.9	12890

improves the shear capacity of the system and transfers the cracks away from the joint. The results are illustrated in Figure (14). Table (3) shows the maximum load carrying capacity and the strength increase percentage for the retrofitted specimens and the base specimen.

6. Conclusions

This paper conducted a comprehensive analytical investigation to evaluate the performance of exterior concrete connections retrofitted using FRP strips and FRP bars through the Near Surface Mounted (NSM) method, offering a practical and cost-effective alternative to fully covering the connection zone with FRP. Numerical models were utilized to analyze various performance metrics, including shear strength, ductility ratio, connection secant stiffness, and plastic strain. The results indicated that employing full overlap of FRP sheets at the beam-column joint effectively prevents the separation of FRP sheets. All the proposed NSM methods significantly improved the flexural capacity of RC beam-column joints. Specifically, the NSM method of embedding CFRP bars within the joint core efficiently transferred forces to the column. Among the retrofitted specimens using FRP strip arrangements, the configuration combining diagonal and orthogonal strips demonstrated the most effective performance, minimizing damages in the joint area and column while redirecting them to the beam. The strip arrangement, with proper anchorage in the wrapping around the connection's circumference in both the beam and column, emerged as a suitable method for retrofitting FRP connections, potentially replacing full FRP laminate coverage. This approach not only increased strength to a desired level but also improved damage distribution within the connection and beam-column assembly, thereby reducing damage in the column. Additionally, retrofitting the connection with FRP strips increased the area under force-displacement curves and enhanced the ductility ratio, promoting maximum plastic strain outside the joint and boosting the joint's energy dissipation capacity. Nonetheless, further investigation is needed on the spacing, number of U-shaped and cross-shaped bars, and varying penetration depths of CFRP bars into the joint core. Implementing these methods in full-scale structures may pose new challenges, necessitating additional research. Numerical studies are recommended to explore the impact of various parameters on the performance of these proposed methods.

Acknowledgements

The authors would like to thank the logistical support provided by the IIEES (International Institute of Earthquake Engineering and Seismology in Tehran, Iran). This work is based upon research funded by Iran National Science Foundation (INSF) under PROJECT No. 4031187.

References

ACI (2019). *ACI 318-19 Building Code Requirements for Structural Concrete and Commentary*. In 318-19 Building Code Requirements for Structural Concrete and Commentary. https://doi.org/10.14359/51716937

Apandi, N.M., Ma, C.K., Chin, C.L., Awang, A.Z., Omar, W., Rashid, A.S.A., & Zailani, W.W.A. (2023). Preliminary pre-damaged level assessment for concrete structures: A review. In *Structures*. https://doi.org/10.1016/j.istruc.2023.05.130

Di Ludovico, M., Balsamo, A., Prota, A., & Manfredi, G. (2008). Comparative assessment of seismic rehabilitation techniques on a full scale 3-story RC

moment frame structure. Structural Engineering and Mechanics. https://doi.org/10.12989/sem.2008.28.6.727

Esmaeeli, E., & Barros, J.A.O. (2015). Flexural strengthening of RC beams using Hybrid Composite Plate (HCP): Experimental and analytical study. *Composites Part B: Engineering*. https://doi.org/10.1016/j.compositesb.2015.05.003

Han, T., Dong, Z., Zhu, H., Wu, G., & Zhao, X. (2023). Compression behavior of concrete columns combinedly confined by FRP externally wrapped Fe-SMA strips. *Engineering Structures*. https://doi.org/10.1016/j.engstruct.2023.116754

Ji, J., Han, T., Dong, Z., Zhu, H., Wu, G., Wei, Y., & Soh, C. K. (2023). Performance of concrete columns actively strengthened with hoop confinement: A state-of-the-art review. *In Structures*. https://doi.org/10.1016/j.istruc.2023.05.038

Kent, D.C., & Park, R. (1971). Flexural members with confined concrete. *Journal of the Structural Division*.

Le-Trung, K., Lee, K., Lee, J., Lee, D. H., & Woo, S. (2010). Experimental study of RC beam-column joints strengthened using CFRP composites. *Composites Part B: Engineering*. https://doi.org/10.1016/j.compositesb.2009.06.005

Mostofinejad, D., & Hajrasouliha, M. (2019). 3D beam-column corner joints retrofitted with X-shaped FRP sheets attached via the EBROG technique. *Engineering Structures*. https://doi.org/10.1016/j.engstruct.2019.01.038

Nateghi-Alahi, F., & Shokrzadeh, M.R. (2019). Behavior considerations for mechanical rebar couplers. *Behavior Considerations for Mechanical Rebar Couplers*, 30-41. https://isn.ac/XBHB-EZGFF

Realfonzo, R., Napoli, A., & Pinilla, J.G.R. (2014). Cyclic behavior of RC beam-column joints strengthened with FRP systems. *Construction and Building Materials*. https://doi.org/10.1016/j.conbuildmat.2013.12.043

Shokrzadeh, M.R. (2017). *Numerical Modeling of Reinforced Concrete Joints Reinforced with FRP in Software ABAQUS*. 2017/1/26, 10-22.

Shokrzadeh, M.R. (2024). *Experimental Study of Seismic behavior and Modification of the Failure Region of Mechanical Bar Splices in Reinforced Concrete Vertical Elements*. Islamic Azad University Science and Research Branch.

Shokrzadeh, M.R., & Aziminejhad, A. (2018). Investigating of the performance of different diagonal brace patterns in rehabilitation Lightweight Steel Frame (LSF). *Analysis of Structure and Earthquake*, *1*(1), 1.

Shokrzadeh, M.R., Aziminejad, A., & Moghaddam, A.S. (2024). Evaluation of various FRP strengthening configurations for RC beam-column joints. *Bridge Structures*, Preprint (Preprint), 1-21. https://doi.org/10.3233/BRS-240223

Shokrzadeh, M., Aziminejhad, A., & Sarvghad-moghaddam, A. (2016). Hysteretic behavior of concrete connections strengthened by X-shape FRP strips. *Analysis of Structure and Earthquake*, *12*(4), 29-40. https://civil-strj.maragheh.iau.ir/article_525485.html

Shokrzadeh, M.R., Nateghi-Alahi, F., Mansoori, M.R., & Javadi, P. (2023). The improvement of the threaded-based mechanical splice by modifying the threaded system: Study of techniques cold rolling and rotating friction welding. *Journal of Building Engineering*, *80*, 107964. https://doi.org/10.1016/J.JOBE.2023.107964

Shokrzadeh, M.R., & Nateghi-Alahi, F. (2022). Evaluation of hybrid NSM-CFRP technical bars and FRP sheets for seismic rehabilitation of a concrete bridge pier. *Bridge Structures*, *18*(3-4), 75-88. https://doi.org/10.3233/BRS-290180

Shokrzadeh, M.R., Nateghi Allahe, F., Mansoori, M. R. & Javadi, P. (2022). Failure area evaluation of the coupler with threaded bar: Experimental and Numerical study. *International Journal of Advanced Structural Engineering*, *12*(1), 531-543. https://doi.org/10.1007/IJASE.2022.692294

Shokrzadeh, M.R., Oveyci, A.M., Pourmirza, R. & Shaifi, M. (2024). Seismic retrofitting of concrete beam-column connections using FRP strip and CFRP bar with NSM technique. *9th International*

Conference on Seismology and Earthquake Engineering (SEE9).

Shrestha, R., Smith, S.T., & Samali, B. (2009). Strengthening RC beam-column connections with FRP strips. *Proceedings of the Institution of Civil Engineers: Structures and Buildings*. https://doi.org/10.1680/stbu.2009.162.5.323

Simulia, & ABAQUS. (2019). *Abaqus User's Manual version 2019. In Dassault Systèmes Simulia Corp.: Providence*, RI, USA.

Sumer, Y. & Aktas, M. (2015). Defining parameters for concrete damage plasticity model. *Challenge Journal of Structural Mechanics*. https://doi.org/10.20528/cjsmec.2015.07.023

Vilanova, I., Torres, L., Baena, M., & Llorens, M. (2016). Numerical simulation of bond-slip interface and tension stiffening in GFRP RC tensile elements. *Composite Structures*, *153*, 504-513. https://doi.org/10.1016/j.compstruct.2016.06.048